THE JOURNAL OF PHYSICAL CHEMISTRY C

pubs.acs.org/JPCC

Article

Adsorbate-Induced Segregation of Cobalt from PtCo Nanoparticles: Modeling Au Doping and Core AuCo Alloying for the Improvement of Fuel Cell Cathode Catalysts

Barbara Farkaš, Christopher B. Perry, Glenn Jones,* and Nora H. de Leeuw*

Cite This: J. Phys. Chem. C 2020, 124, 18321−18334

Read Online

ACCESS | Metrics & More | Article Recommendations

ABSTRACT: Platinum, when used as a cathode material for the oxygen reduction reaction, suffers from high overpotential and possible dissolution, in addition to the scarcity of the metal and resulting cost. Although the introduction of cobalt has been reported to improve reaction kinetics and decrease the precious metal loading, surface segregation or complete leakage of Co atoms causes degradation of the membrane electrode assembly, and either of these scenarios of structural rearrangement eventually decreases catalytic power. Ternary PtCo alloys with noble metals could possibly maintain activity with a higher dissolution potential. First-principles-based theoretical methods are utilized to identify the critical factors affecting segregation in Pt−Co binary and Pt−Co−Au ternary nanoparticles in the presence of oxidizing species. With a decreasing share of Pt, surface segregation of Co atoms was already found to become thermodynamically viable in the PtCo systems at low oxygen concentrations, which is assigned to high charge transfer between species. While the introduction of gold as a dopant caused structural changes that favor segregation of Co, creation of CoAu alloy core is calculated to significantly suppress Co leakage through modification of the electronic properties. The theoretical framework of geometrically different ternary systems provides a new route for the rational design of oxygen reduction catalysts.

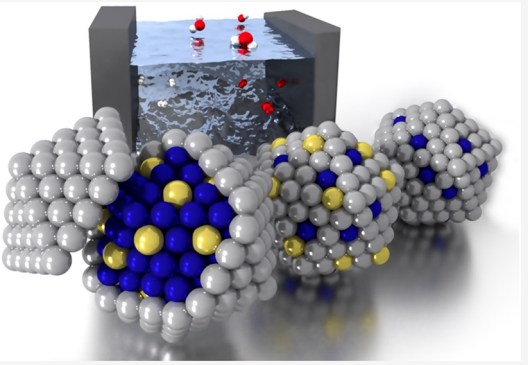

1. INTRODUCTION

Fuel cells are gaining importance in efficient power generation schemes, owing to their high efficiency and unlimited sources of environmentally sustainable reactants, thus providing a cost-effective supply of power which could amplify the emerging hydrogen economy. They combine the best features of engines and batteries, operating as long as fuel is available without any intermediate mechanical energy conversion (similar to an engine), while converting chemical energy of fuel and oxidant into electric energy without the need to recharge (resembling batteries under load conditions).[1] Among the range of fuel cell technologies available, proton exchange membrane (PEM) fuel cells have the advantages of simplicity, quick start-up, high power density and thermodynamic efficiency, which, when combined with the low operating temperatures (<100 °C), make them a promising alternative to devices that are currently employed in transportation applications.[2] Nevertheless, it has been generally accepted that the advantages offered by PEM fuel cells still have to be furtherly commercialized to address production expenses, environmental concerns, energy security, and hydrogen storage.[3−5] Cost, durability, and overpotential, described in more detail below, were identified as the main limitations, and methods for their enhancement are constantly being investigated to enable PEM fuel cell technology to become viable on the market.

In PEM fuel cells, protons released by hydrogen oxidation at the anode move through a solid polymer electrolyte membrane to the cathode, where they meet supplied oxygen and electrons transferred through the circuit, resulting in the electrocatalytic oxygen reduction reaction (ORR) with water as the final product.[6] This rate-limiting reaction that takes place at the cathode currently constrains the operating efficiency to 40−45% as a result of several obstacles which need to be overcome before large-scale implementation. A major drawback is the fact that costly platinum, as the metal with the highest activity for ORR, makes PEM fuel cells too expensive for widespread adoption. The development of nanoparticle (NP) Pt catalysts has considerably reduced the metal loading, but, regardless of the high ORR activity, the kinetics of the reaction is still unfavorable, resulting in the high overpotential required, which

Received: May 18, 2020
Revised: June 22, 2020
Published: June 23, 2020

Table 1. Lattice Parameters and Heats of Mixing for PtCo and AuCo Alloys of Different Compositions Calculated within the PBE and rPBE Functionals and Available Experimental Data on the Same Systems

		Pt_3Co	PtCo	$PtCo_3$	$Au_{87}Co_{13}$
a (Å)	this work PBE	3.883	3.797	3.652	4.131
	this work rPBE	3.907	3.822	3.692	4.130
	DFT[42,43]	3.90	3.83	3.67	
		3.89	3.78		
	exp[44−46]	3.854	3.803	3.664	
ΔH_{mix} (kJ mol^{-1})	PBE	−10.23	−12.18	−8.01	+8.68
	rPBE	−22.29	−20.45	−12.74	+14.00
	exp[47−49]	−9.2 − −12.0	−9.8 − −14.0	−7.0 − −7.5	+5.3

limits application of cathodes that rely on this precious metal as a catalyst.[7,8]

There has been significant focus on the search for catalysts with increased activity and reduced price to make low-temperature fuel cells more economically attractive.[9] A promising solution, without losing the advantages of Pt nanoparticles, are core−shell NPs in which the core is composed of nonprecious metal with an outer platinum shell.[10−12] Alloying of platinum with transition metals has been extensively reported to decrease the binding energy of relevant ORR species, due to the modifications in the geometry and electronic structure induced by the strain and/or ligand effects of the underlying transition metal,[13−15] and similar properties have been observed for the nanoscale systems.[16] These changes, in turn, decrease the onset potential for water oxidation and increase the working potential, thus enhancing the overall efficiency of the cell. Not only does a lower binding energy improve ORR activity making bulk and nanoalloys superior to standard Pt systems, but addition of other metals also makes the cathode more cost-effective. In this respect, PtCu,[17] PtNi,[18,19] and PtCo[12,20−22] combinations have been reported as especially effective alloy and NP candidates. Recent progress on nanoscale has also been made using near-surface alloys, with one such promising geometry being a monolayer Pt shell overlaying a random alloy core of variable composition.[23,24] So-called alloy−core@shell nanoparticles have shown both the robustness of core−shell structures and the tunability of random alloy particles.[25]

However, the introduction of transition metal atoms in Pt alloys has limitations because they can easily segregate due to a lattice mismatch or difference in the surface energy.[26] In the presence of ORR intermediates, this phenomenon can be accelerated owing to the strong interaction of transition metals with oxygen species.[8,27−29] Not only would the intense interaction caused by this surface segregation hinder the mechanism of the ORR, but many of these metals could additionally damage the membrane of the fuel cell if they leak from the catalyst over the lifetime of the cell.[21] The initial enhancement of activity might therefore be offset by degradation of the membrane electrode assembly and contamination of the ion-exchange sites in the membrane. Stabilization of such systems remains a challenge, owing to the extremely corrosive environment at the cathode. Despite showing improved ORR activity, most of the cubic-structured Pt-transition metal alloys studied thus far are not known to efficiently stabilize the secondary metal under the acidic fuel cell conditions. Preventing the segregation and leakage of the transition metal atoms is crucial for the successful improvement of ORR catalysts and their implementation in fuel cells.[30]

Ternary Pt alloys and NPs are offering both the potential for fine-tuning of the electronic structure and improving the resultant catalytic activity, in addition to being a possible structural solution to prevent transition metal leakage.[31] Ternary octahedral Pt−Ni-based nanoparticles, such as Pt−Ni−Fe and Pt−Ni−Cu NPs, characterized by high activity and promising stability for the ORR, were recently described.[32] Owing to the excellent catalytical properties of both Pt−Ni and Pt−Co bimetallic systems, ternary Pt−Ni−Co NPs have also attracted much attention, with precise control over the composition, size, and phase of the nanoparticles during synthesis and subsequent treatment identified as being crucial for their electrocatalytic activity and stability.[33,34] Most of the combinations, however, still experience transition-metal leakage, and addition of noble metals with higher dissolution potentials has proved to be a useful strategy.[35] A recent synthesis of PtCo NPs with added Au showed improved durability by weakening the binding energy of surface oxygen species and suppressed Co surface segregation.[36] It has also been experimentally confirmed that introducing Au or Ag to the Pd core can enhance the stability and durability of a Pt surface layer of PtPd NPs under ORR conditions.[25]

Hence, addition of the third metal provides a potentially facile way to enhance the activity and durability of the electrode catalyst for PEM fuel cell application. This tuning mechanism is a general property of the ternary nanoparticles, with alloy−core@shell systems expanding the potential possibilities, and it therefore provides systematic means to design nanoparticles with desirable stability and catalytic activity. A direct comparison between the Pt-transition metal NPs doped with a ternary metal and the alloy−core@Pt shell NPs has not yet been carried out. The correlation between electronic structure and surface segregation behavior, which is fundamental to achieve the desired catalyst properties, still remains elusive for such multimetallic systems. Identification of the phenomena that are responsible for the changes in the structure and activity of multielement nanoparticles is by no means easily achievable experimentally. Therefore, theoretical investigations of such complicated systems can reveal the critical factors behind the environmentally driven dynamic structural evolution and, hence, form the basis for the rational design of new catalysts.

Herein, results from density functional theory (DFT) calculations that were carried out to provide detailed insight into the role of gold in the stabilization of Co leakage from PtCo bimetallic NPs of varying compositions are presented. Since the mechanisms that underlie the segregation phenomena highly depend on the presence of the oxidizing adsorbates, the stability of the systems under conditions, where oxygen chemisorption is anticipated, was tested to determine if there is

https://dx.doi.org/10.1021/acs.jpcc.0c04460
J. Phys. Chem. C 2020, 124, 18321−18334

any adsorbate-induced structural transformation affecting the electrochemical stability. In addition, the difference between gold doping and gold−cobalt core alloying has been explored.

2. COMPUTATIONAL DETAILS

Spin-polarized density functional theory calculations were conducted using the Vienna Ab Initio Simulation Package (VASP) code[37] within the generalized gradient approximation (GGA) of the exchange-correlation functional developed by Perdew, Burke, and Ernzerhof (PBE).[38] The rPBE functional, which is commonly used in heterogeneous catalysis for its improved description of adsorbate−metallic surface interactions,[39,40] was found to significantly overestimate the heat of mixing, which is a useful indicator of alloying between the considered metals, Table 1. A similar trend was reported for PtNi alloys.[41] Therefore, to properly capture segregation properties within the doped and core-alloyed bi- and trimetallic NPs in this study, the appropriate description of metal−metal interactions was prioritized at the price of accuracy of adsorption energies, and the PBE functional was therefore employed in this work.

The core electrons up to and including the 3p levels of cobalt and 5p levels of platinum and gold were kept frozen and their interaction with the valence electrons was described by the projector augmented wave (PAW) method.[50] The DFT-D3 method with Becke-Johnson damping was used for the addition of the long-range dispersion interactions.[51] Kohn−Sham orbitals were expanded by plane waves up to a cutoff energy of 400 eV, and the Monkhorst−Pack k-point grid included only Γ-point to sample the Brillouin zone of each nanoparticle. Structural optimizations were carried out with the conjugate gradient (CG) algorithm without any constraints, with the convergence criteria for the change in the total energy and interatomic forces between two steps set at 1.0×10^{-6} and 1.0×10^{-2} eV/atom, respectively. The vacuum space in the unit cell was set to be more than 12 Å in each direction to avoid interactions with the neighboring nanoparticles.

2.1. Energetics. The relative stabilities of NPs were analyzed through their mixing energies, E_{mix},[52,53] which can be calculated for mixed systems with respect to their parent NP end-members as

$$E_{mix} = \frac{1}{m+n}\left[E(A_mB_n) - \frac{m}{m+n}E(A_{m+n}) - \frac{n}{m+n}E(B_{m+n})\right] \quad (1)$$

where $E(A_mB_n)$, $E(A_{m+n})$, and $E(B_{m+n})$ are the calculated DFT energies of bimetallic A_mB_n and monometallic A_{m+n} and B_{m+n} nanoparticles with $m + n$ atoms. From this definition, negative (positive) mixing energies indicate energetically favorable (unfavorable) NP formation.

To investigate whether adsorbed oxygen atoms induce surface segregation of the core element, the surface segregation energy, ΔE_{seg}, was defined as

$$\Delta E_{seg} = E_{NPsegregated} - E_{NPinitial} \quad (2)$$

where $E_{NPinitial}$ and $E_{NPsegregated}$ are the respective DFT energies before and after surface segregation. The less positive the ΔE_{seg}, the easier the surface segregation. Adsorption energies, E_{ads}, of oxygen were calculated as

$$E_{ads} = \frac{1}{n}\left[E_{NP+nO} - E_{NP} - n\frac{1}{2}E_{O_2}\right] \quad (3)$$

where E_{NP+nO}, E_{NP}, and E_{O_2} are the calculated DFT energies of a NP with n adsorbed oxygen atoms, a bare NP, and the oxygen molecule, respectively. Well-known overbinding of O_2 molecule by PBE was considered,[54,55] and the employed E_{O_2} was corrected accordingly, by subtracting the empirically measured energy reported in thermochemical tables[56] from the DFT calculated energy. An overbinding energy of −0.86 eV was thereby detected, giving a correction of −0.43 eV per oxygen atom. Charge distribution was calculated using the Bader charge analysis, as implemented by Henkelman et al.[57]

2.2. Model Systems. Theoretical studies of the effect of transition-metal doping or integration into core−shell NPs are often placed in the framework of bilayer slab models for simplicity of calculations.[58] This simplification is governed by two assumptions: first, the surface chemistry of the NP is dominated by the first two or three atomic layers, and second, chemistry of crystal facets of the NPs can be approximated by their respective single crystal surfaces. While such models can approximately resemble large particles with an appreciable share of facet areas, results obtained from extended slabs may not represent a realistic picture for NP systems, especially when it comes to NPs of a few nanometres in diameter. In such cases, the non-negligible portion of chemically under-saturated sites (steps, edges, vertices), which are naturally more reactive, creates a distinguishable difference in the catalytic activity and triggered structural changes of nanoscale entities. Considering that the average size of catalyst particles in commercial fuel cells is not larger than a few nanometres, it is important to understand this simultaneous effect of size and surface structure. To mimic experimental systems as closely as possible, in this study the evaluation of phenomena that describe the dynamical behavior of NPs was performed within cluster models.

2.2.1. Size. As the nanoparticle size decreases, the distribution of surface terraces and low coordination sites changes in favor of the latter. Due to much stronger oxygen binding on undercoordinated sites of the smaller NPs,[59,60] the corresponding ORR activity is expected to be lowered. For example, for small Pt NPs, catalytic activity was experimentally observed to be adversely affected by size in the 1 to 5 nm range, with a sharp decline in the ORR activity when going toward 1 nm and a peak of mass activity displayed between 2 and 2.5 nm in diameter; similar conclusions have been drawn from theoretical calculations.[61−65]

Significant changes in the ORR activities of Pt binary NPs, which are 3−10 times higher than that of pure Pt,[19,20] are also reflected in the size of NPs. A sharp contrast in size dependence of the activity was revealed between PtCo/C and PtNi/C catalysts in the size range from 1.5 to 9 nm, with a subtle increase in activity for PtNi/C and a maximum for sizes between 6 and 7 nm, while PtCo/C catalysts showed a clear trend of decrease in activity with increasing particle size, peaking at the smallest sizes just above 2 nm in diameter.[18] Additionally, PtCo NPs of different compositions have already been synthesized and tested for satisfactory ORR activity within the 1.5−3.0 nm range.[66,67]

Here, a magic number 147 atom cluster has been chosen as a representative model for PtCo catalyst system as it offers three levels to study the segregation events−core (central atom with surrounding first shell), subshell, and shell. With its diameter between 1.5 and 2.0 nm, the size is within the lower limit of

https://dx.doi.org/10.1021/acs.jpcc.0c04460
J. Phys. Chem. C 2020, 124, 18321−18334

Table 2. Mixing Energies, E_{mix}, and Energies of Segregation per Co Atom (Overall in Parentheses), ΔE_{seg}, of 1, 13, and 20 Cobalt Atom Segregation in the 147 Atom PtCo NPs of Different Compositions[a]

		$Pt_{134}Co_{13}$	$Pt_{117}Co_{30}$	$Pt_{92}Co_{55}$
E_{mix}		−0.073	−0.180	−0.260
ΔE_{seg}	1 Co	0.492	0.685	0.146
	13 Co	0.891 (11.585)	0.936 (12.162)	0.478 (6.212)
	20 Co		0.908 (18.157)	0.538 (10.756)

[a]All energies are expressed in eV.

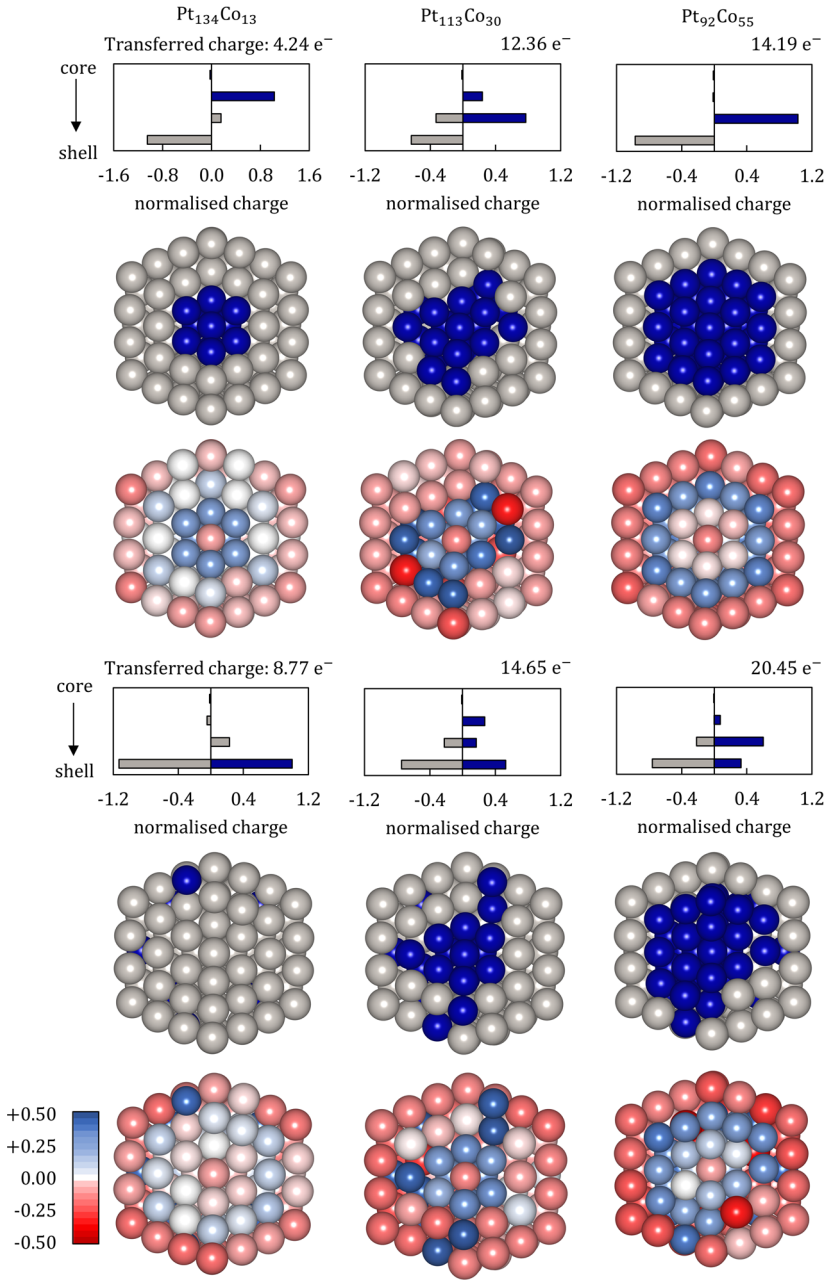

Figure 1. Effect of composition on charge distribution in PtCo core−shell NPs before (top panel) and after (bottom panel) segregation of 13 Co atoms. Top of each panel: layer-by-layer net charge distributions. The charges have been normalized by the total amount of charge transferred from Pt to Co, which is particle dependent and listed above each graph. Negative charges indicate an electron excess. At the bottom of the panels, cross sections of the nanoparticles demonstrating inhomogeneous distribution of charge onto individual atoms, with the actual atomic structure given for reference in the middle. Note: only a single atomic plane is visible in the cross sections, whereas all atoms are included in the layer-by-layer averaging. Blue spheres and bars represent cobalt atoms and their transferred charges, whereas gray spheres and bars represent platinum atoms and their transferred charges. Legend for charge distribution is given on the bottom left in e^-.

https://dx.doi.org/10.1021/acs.jpcc.0c04460
J. Phys. Chem. C 2020, 124, 18321−18334

NP systems used in experimental studies and can be modeled at affordable computational price.

2.2.2. Shape. The stability of pure 1−2 nm Pt NPs, considering dissolution and coalescence, was found to be highly shape dependent. While octahedral NPs showed superior stability against dissolution, their oxygen adsorption strength is too low for ORR applications. In terms of coalescence, icosahedron and cuboctahedron are the most stable shapes, with the former allowing for the maximum relaxation of Pt atoms on carbon support. When combined with transition metals in the form of core−shell NPs, together with the improvement in the ORR activity, better stability against both dissolution and coalescence was obtained within an icosahedral architecture.[68]

Theoretical studies have also sampled octahedral, cuboctahedral, and icosahedral shapes to identify the most stable configuration of small PtCo NPs as a function of particle size and composition. The icosahedron has been shown to be the most stable shape regardless of the size or composition, with small distortions in certain cases.[22,69] Therefore, model within this study is based on a 147 atom icosahedral NP composed of only (111) facets, which have also shown better ORR reactivity compared to other fcc surfaces.

2.2.3. Ordering. Thermodynamically, PtCo NPs indicate a strong core-region preference for Co both experimentally and theoretically. This behavior can be explained by the smaller atomic radius of Co and higher surface energy of Co (0001) and Co (111) surfaces compared to the Pt (111) surface, which favors Pt atoms in the outer shells to minimize the total surface energy of the NP. In addition, the large segregation energy of a single Co atom impurity from core to the surface of the Pt NP further shows the energetic unfavorability of cobalt occupying the surface sites.[22,70]

To investigate the effect of composition of PtCo NPs on segregation, three 147 atom icosahedron core−shell model systems were created: $Pt_{134}Co_{13}$, $Pt_{117}Co_{30}$, and $Pt_{92}Co_{55}$ with ∼10, 20, and 35% of cobalt, respectively. Afterward, gold was introduced as a dopant in the subshell of the $Pt_{134}Co_{13}$ system and shell of $Pt_{92}Co_{55}$. To compare doping with core-alloying, gold was also added to the core of the $Pt_{92}Co_{55}$ system in different Co−Au ratios (∼15, 25, and 35% of gold).

3. RESULTS AND DISCUSSION

3.1. Composition-Dependent Segregation Energy of Bimetallic PtCo Nanoparticles. The effect of cobalt concentration on the segregation behavior has first been tested in the absence of adsorbates. The energy needed for segregation of a single cobalt atom, 13 cobalt atoms, and 20 cobalt atoms to the (111) facets of the NPs has been estimated from two DFT calculations: (i) for the initial structure with all cobalt atoms in the core of the nanoparticle ($Co_{in\text{-}core}$), and (ii) for the homotop where one or more cobalt atoms are occupying the terrace facet sites in the outer shell of the NP (Co_{terr}). The 13 cobalt atom segregation represents segregation of all cobalt atoms of the $Pt_{134}Co_{13}$ system and is performed for the other two compositions to allow direct comparison, whereas the 20 cobalt atom segregation makes terrace sites of all (111) icosahedral planes taken by cobalt atoms. In all cases, cobalt atoms are placed in the middle of the (111) facet as it is the energetically preferred site for single Co atom segregation. Results are shown in Table 2 for the three compositions considered.

Table 3. Adsorption Energies, E_{ads}, and Average Metal−Oxygen Distances, $\bar{d}_{M-O}$, for Single O Atom Adsorption in Various Adsorption Sites of the Pt_{147} NP and $Pt_{134}Co_{13}$ NP with 12 Cobalt Atoms in the Core and One Cobalt Atom in the (111) Terrace[a]

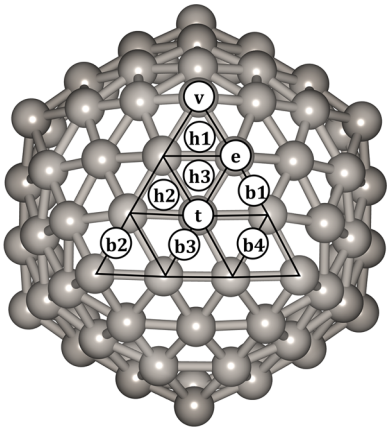

	Pt_{147}		$Pt_{134}Co_{13}$	
adsorption site	E_{ads} (eV)	$\bar{d}_{Pt-O}$ (Å)	E_{ads} (eV)	$\bar{d}_{M-O}$ (Å)
vertex (v)	−1.64	1.78	−1.64	1.77
edge (e)	−1.12	1.80		
top (t)	−0.94	1.81	−1.46	1.62
bridge 1 (b1)	−1.94	1.93	−1.89	1.93
bridge 2 (b2)	−1.92	1.96	−1.85	1.96
hollow 1 (h1)	−1.94	2.03	−1.97	2.07
hollow 2 (h2)	−1.86	2.07	**−2.29**	1.85
hollow 3 (h3)	**−1.98**	2.05	−2.21	1.86

[a]The most favorable adsorption energy is represented in bold.

The thermodynamic stability of the structures considered is an important factor if the nanoparticle is to function as a catalyst. Stabilities of the $Pt_{134}Co_{13}$, $Pt_{117}Co_{30}$, and $Pt_{92}Co_{55}$ NPs were quantified through the values of their mixing energies. All three compositions have negative mixing energies per atom, Table 2, with the $Pt_{92}Co_{55}$ NP, where core sites and all inside shells are occupied by cobalt atoms with a single overlayer of platinum, showing the most favorable mixing behavior with E_{mix} of −0.260 eV per atom.

For the $Pt_{134}Co_{13}$ system, where cobalt atoms occupy the core site and the entire first shell, the segregation energy of a single Co atom equals 0.492 eV. For all 13 cobalt atoms to segregate to the facets of the outer shell, the segregation energy required per atom at 0.891 eV is almost double that of the single cobalt atom. In the case of cobalt atoms fully occupying both core and subshell in the $Pt_{92}Co_{55}$ NP, the segregation energy of the single Co atom is substantially lower at 0.146 eV. For 13 (111) terrace sites to be occupied by cobalt atoms, an energy of 0.478 eV per atom would be required, which is about half the energy needed for the same process to occur in the $Pt_{134}Co_{13}$ system. The intermediate composition, $Pt_{117}Co_{30}$, where the number of cobalt atoms is insufficient to completely populate the subshell, has the highest energetic costs for segregation of any number of cobalt atoms to the outer shell, with 0.685 eV for the segregation energy of a single Co atom and 0.936 eV for the segregation energy per Co atom for the 13 atom segregation.

The origin of the difference in the segregation behavior of NPs with varying compositions can be traced to their electronic structures. Figure 1 illustrates the changes in the

https://dx.doi.org/10.1021/acs.jpcc.0c04460
J. Phys. Chem. C 2020, 124, 18321−18334

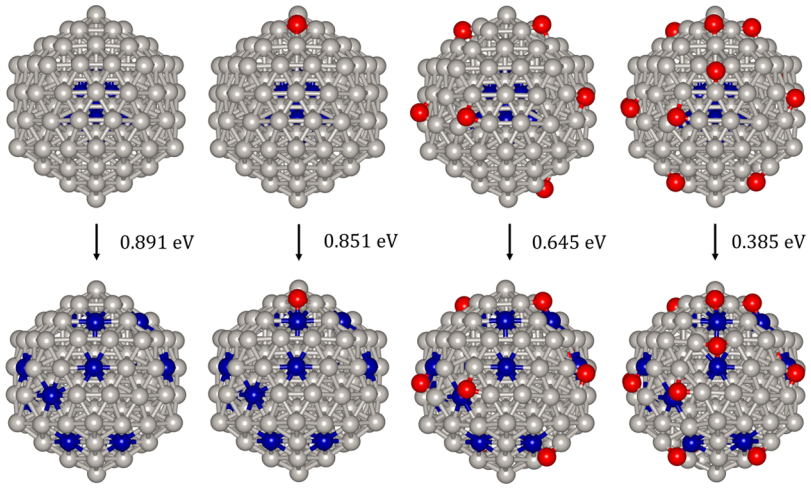

Figure 2. Structures of $Pt_{134}Co_{13}$ NP $Co_{in\text{-}core}$ (top row) and Co_{terr} (bottom row) homotops with O adsorbates in hollow sites (0, 1, 10, and 13 O atoms from left to right, respectively). The corresponding segregation energies, ΔE_{seg}, are given in eV per Co atom. Gray, blue, and red spheres represent Pt, Co, and O atoms, respectively.

Table 4. Energies of Segregation per Co Atom (Overall in Parentheses) of 13/20 Cobalt Atoms from Core Sites to (111) Terraces for Three NP Compositions, $Pt_{134}Co_{13}$, $Pt_{117}Co_{30}$, and $Pt_{92}Co_{55}$, after Adsorption of One, ΔE_{seg+O}, 10, $\Delta E_{seg+10\ O}$, and 13/20, $\Delta E_{seg+13/20\ O}$, Oxygen Atoms[a]

	13 Co			20 Co		
	ΔE_{seg+O}	$\Delta E_{seg+10\ C}$	$\Delta E_{seg+13\ C}$	ΔE_{seg+O}	$\Delta E_{seg+10\ O}$	$\Delta E_{seg+20\ O}$
$Pt_{134}Co_{13}$	0.851 (11.064)	0.492 (6.398)	0.385 (5.005)			
$Pt_{117}Co_{30}$	0.902 (11.721)	0.417 (5.416)	0.244 (3.174)	0.877 (17.548)	0.520 (10.397)	0.135 (2.706)
$Pt_{92}Co_{55}$	0.422 (5.492)	−0.093 (−1.208)	−0.345 (−4.484)	0.494 (9.650)	0.173 (3.451)	−0.261 (−5.215)

[a]All energies are expressed in eV.

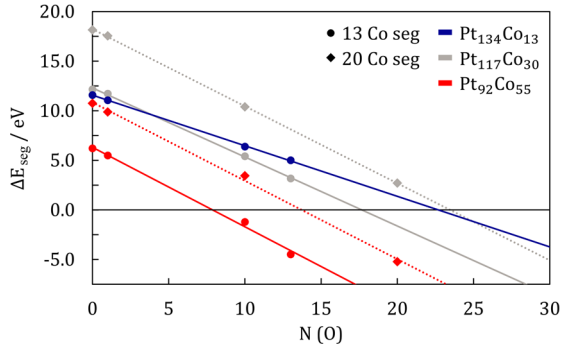

Figure 3. ΔE_{seg} for segregation of 13 (circle) and 20 (diamond) Co atoms of $Pt_{134}Co_{13}$ (blue), $Pt_{117}Co_{30}$ (gray), and $Pt_{92}Co_{55}$ (red) NPs calculated as a function of number of oxygen atoms, N (O), adsorbed. Linear approximations are represented as full and dotted lines.

distribution of excess charge with the variation in composition of bimetallic PtCo NPs before and after the 13 Co atom segregation. Clearly, the charge is not equally divided among atoms within the same layer but accumulates onto the atoms which are coordinated to a greater number of foreign atoms. With only a single Pt shell layer in the $Pt_{92}Co_{55}$ system, practically all of the transferred charge is contained at the interface and atoms of the outer shell bear considerable negative charge gained from underneath cobalt atoms. For the $Pt_{134}Co_{13}$ composition with a double Pt layer, the outer shell is still negatively charged but this time due to both gain from the cobalt atoms and the flow of electrons from the underlying Pt layer toward the Pt−vacuum interface. The $Pt_{117}Co_{30}$ system with a subshell composed of both Pt and Co atoms contains most of the charge on the few atoms that experience a drastic change in the environment caused by this composition. The negative charge of the outer Pt shell is lessened, but the overall charge transfer from Co to Pt is only 1.83 e^- less compared to the $Pt_{92}Co_{55}$ system, even though the total number of Co atoms is lower by 25. Additionally, less positive charge on segregated cobalt atoms in the $Pt_{92}Co_{55}$ composition is an indicator that higher reactivity toward oxygen could be expected compared to the other two systems.

3.2. Screening of Single O Adsorption on Terraces of Bimetallic PtCo Nanoparticles. In the presence of adsorbates that can bind through oxygen atoms, surface segregation of cobalt in PtCo NPs may become favored due to stronger interactions of Co with adsorbed species. The central question for the present study is what coverage of oxygen would suffice to cause spontaneous segregation of 13 or 20 Co atoms to the surface of PtCo NPs. Coverages are expressed as the number of O atoms adsorbed in respect to the total number of Pt/Co atoms on the surface of the NP ($\theta = N(O)/92$).

With the intention of studying the changes in the segregation energy with the adsorption of atomic oxygen, the adsorption site which is most likely to be observed was probed via adsorption of a single O atom on the pure Pt_{147} NP and on the $Pt_{134}Co_{13}$ NP with one cobalt atom segregated to the (111) terrace. The adsorption sites and accompanying calculated energetic and structural parameters are presented in Table 3. On the pure Pt NP, hollow positions show the most negative adsorption energies, with the h2 site, which includes two Pt atoms of the same edge, having an adsorption energy that is less favorable by about 0.10 eV due to structural constrains.

https://dx.doi.org/10.1021/acs.jpcc.0c04460
J. Phys. Chem. C 2020, 124, 18321−18334

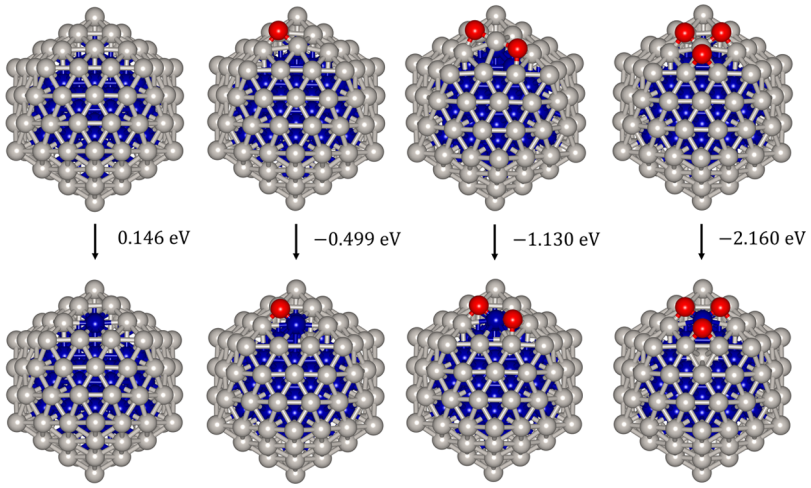

Figure 4. Structures of $Pt_{92}Co_{55}$ NP $Co_{in\text{-}core}$ (top row) and Co_{terr} (bottom row) homotops with multiple O atoms adsorbed per segregated Co atom (zero, one, two, and three O atoms from left to right, respectively). The corresponding segregation energies, ΔE_{seg}, are given in eV. Gray, blue, and red spheres represent Pt, Co, and O atoms, respectively.

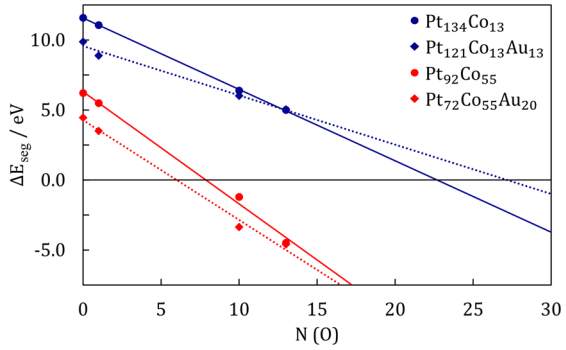

Figure 5. ΔE_{seg} calculated as a function of number of oxygen atoms, N (O), adsorbed on PtCo NPs of different compositions, $Pt_{134}Co_{13}$ (blue) and $Pt_{92}Co_{55}$ (red), without (circle) or with Au doping (diamond). Linear approximations are represented as full and dotted lines.

Adsorption of oxygen on top of a single Pt atom led to considerably weakend interaction, especially for the middle terrace site (t) which is more than 1.00 eV less favorable compared to the hollow (h3) site. Oxygen atoms that were initially adsorbed in b3 and b4 bridge positions spontaneously moved to the closest hollow during relaxation. The presence of a single Co atom on the terrace of the (111) facet has little or no influence on the adsorption energy when the oxygen atom is not directly bonded to cobalt itself, such as in vertex (v), b1, b2, and h1 sites. However, the interaction of oxygen with the NP in sites which include the Co atom is stronger by approximately 0.30−0.50 eV, with hollow sites (h2 and h3) still showing a significant preference over top (t) position. Oxygen that was initially positioned above an edge (e) Pt atom migrated to the closest hollow position (h2) to gain a direct interaction with Co. Evidently, the principal factor for strengthening of the interaction of bimetallic PtCo NPs with oxygen is the availability of Co atoms on the surface of the NP. Since the adsorption in a 3-fold hollow is known to be the most favorable on both Co and Pt surfaces at a low coverage,[71,72] it is not surprising that the hollow site is also dominant in the presence of both species. As the adsorption in the two hollows, h2 and h3, is by far the most favored and since their adsorption energies differ by less than 0.10 eV, further adsorption calculations have been conducted within either of the two sites and no special attention has been given to the ratio of the adsorbate atoms positioned in different hollows for cases with higher numbers of oxygen atoms.

To test the effect of oxygen adsorption on the transition of cobalt to the outer shell for different NP compositions, one O atom has been adsorbed in the most favorable adsorption site (either hollow h2 or h3) close to a single segregated Co atom for the three systems considered. Upon adsorption, the segregation energy for one Co atom in the (111) terrace reduced from a starting value of 0.492 eV to only 0.067 eV for the $Pt_{134}Co_{13}$ system and from 0.685 to 0.365 eV for the $Pt_{117}Co_{30}$ composition. Introduction of oxygen has, therefore, made the segregation more likely to occur in both systems. The biggest change, however, was observed for the system with a single Pt shell, $Pt_{92}Co_{55}$, where the initially low segregation energy of 0.146 eV became exothermic at a value of −0.499 eV.

Already from these tests some estimates of the number of O atoms required to spontaneously trigger full segregation of 13 Co atoms to the surface of bimetallic PtCo NPs can be derived. Given that the energy difference between the two homotops of the PtCo NPs considered here, i.e., $Co_{in\text{-}core}$ and Co_{terr} in the $Pt_{134}Co_{13}$, $Pt_{117}Co_{30}$, and $Pt_{92}Co_{55}$ systems, is 11.585, 12.162, and 6.212 eV, respectively, and the adsorption of O in the hollow as the most favorable adsorption site decreases the segregation energy of one Co atom by 0.425, 0.320, and 0.645 eV, respectively, the approximate number of oxygen atoms needed to segregate 13 Co atoms can be provisionally determined. Accordingly, the adsorption of 27 O atoms (∼0.29 ML) should be sufficient to stabilize the Co_{terr} homotop for the $Pt_{134}Co_{13}$ NP, but only 10 O atoms (∼0.11 ML) for the $Pt_{92}Co_{55}$ NP, and due to the highest difference of homotop energies and the lowest contribution of the oxygen adsorption in reducing the segregation energy, 38 O atoms (∼0.41 ML) are required for the $Pt_{117}Co_{30}$ NP. For the $Pt_{92}Co_{55}$ system, this number is less than one O atom for every Co atom segregated, while it is almost three O atoms per Co for the $Pt_{117}Co_{30}$ system. To develop these estimates on a more systematic basis, adsorption of increased numbers of O atoms has been carried out systematically on two homotops for all three NP compositions.

https://dx.doi.org/10.1021/acs.jpcc.0c04460
J. Phys. Chem. C 2020, 124, 18321−18334

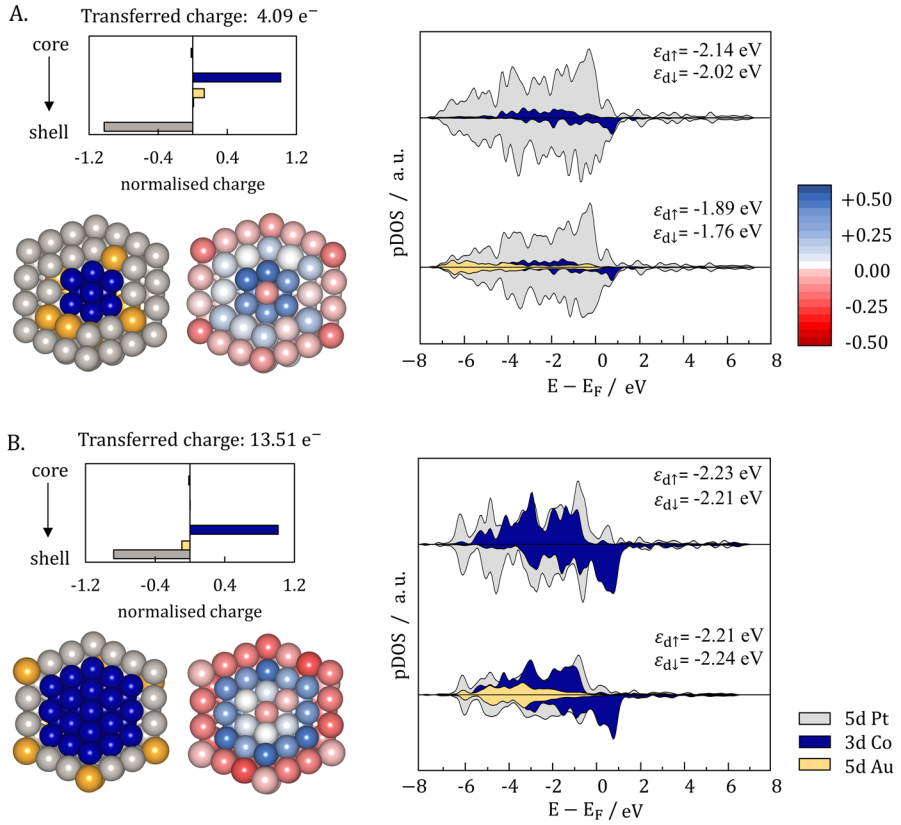

Figure 6. Charge distributions and projected density of state (in a.u.) for (A) $Pt_{121}Co_{13}Au_{13}$ and (B) $Pt_{72}Co_{55}Au_{20}$. For a detailed description of charge analysis, see Figure 1. Top and bottom row of each pDOS panel is for undoped and doped systems, respectively; accompanying d-band center energies are listed in top right corners. Gray, blue, and yellow atoms represent platinum, cobalt, and gold atoms. Legends for charge distribution (in e^-) and pDOS are the same for both A and B.

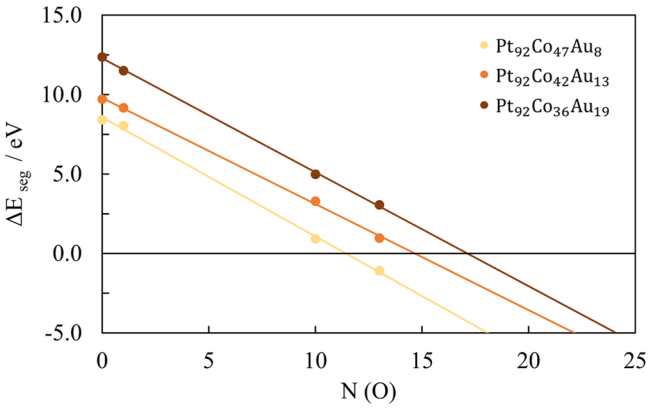

Figure 7. ΔE_{seg} calculated as a function of number of oxygen atoms, N (O), adsorbed on $Pt_{92}(CoAu)_{55}$ NPs with different percentage of Co−Au core alloying (15% Au yellow, 25% Au orange, 35% Au brown). Linear approximations are represented as dotted lines.

3.3. Determination of Threshold Oxygen Concentration to Stabilize Co_{terr} Homo-Top. In the previous section, a rough estimate of the quantity of O atoms needed to pull 13 Co atoms to the surface of PtCo NPs was given. To verify this estimate, O adsorption was explicitly calculated on two homotops, $Co_{in\text{-}core}$ and Co_{terr}, by gradually increasing the number of adsorbate atoms from one to 10 to 13 (20 for 20 Co atom segregation), as shown in Figure 2. This corresponds to oxygen coverages of 0.01, 0.10, 0.15, and 0.20 ML, respectively. Based on the analysis of oxygen binding at different sites, O atoms were randomly adsorbed in h2 and h3 3-fold positions. For each of the considered O systems, the energy difference between the two homotops, ΔE_{seg}, was calculated and the final energies are summarized in Table 4.

Adsorption of just one O atom decreases the energy difference between the homotops by approximately 0.50 eV for all three systems. With 10 adsorbed O atoms, the ΔE_{seg} of 13 Co atoms is calculated to be 6.398, 5.416, and −1.208 eV for $Pt_{134}Co_{13}$, $Pt_{117}Co_{30}$, and $Pt_{92}Co_{55}$ NP, respectively, considerably less than the segregation energies without oxidizing species. When one O atom per segregated cobalt atom is adsorbed, the ΔE_{seg} has decreased further, with final 13 Co atom segregation energies of 5.005 eV for $Pt_{134}Co_{13}$, 3.174 eV for $Pt_{117}Co_{30}$, and −4.484 eV for $Pt_{92}Co_{55}$ system. The negative sign implies that surface segregation of Co became energetically favorable. To obtain the threshold coverage of oxygen for stabilization of the Co_{terr} homotop, ΔE_{seg} has been plotted as a function of the N(O) adsorbed in Figure 3. The calculated dependence is well approximated linearly, and the number of oxygen atoms needed for spontaneous segregation of 13 Co atoms in $Pt_{134}Co_{13}$, $Pt_{117}Co_{30}$, and $Pt_{92}Co_{55}$ NP is 23 (~0.25 ML), 18 (~0.20 ML), and 8 (~0.09 ML), in that order. For segregation of 20 Co atoms in $Pt_{117}Co_{30}$ and $Pt_{92}Co_{55}$ systems, N(O) corresponds to 24 (~0.26 ML) and 14 (~0.15 ML). These numbers agree well with the estimates proposed earlier, but only for the two completely core−shell systems. In the $Pt_{117}Co_{30}$ composition, the number of oxygen atoms required was significantly overestimated, because every cobalt atom segregated to the surface has a different

https://dx.doi.org/10.1021/acs.jpcc.0c04460
J. Phys. Chem. C 2020, 124, 18321−18334

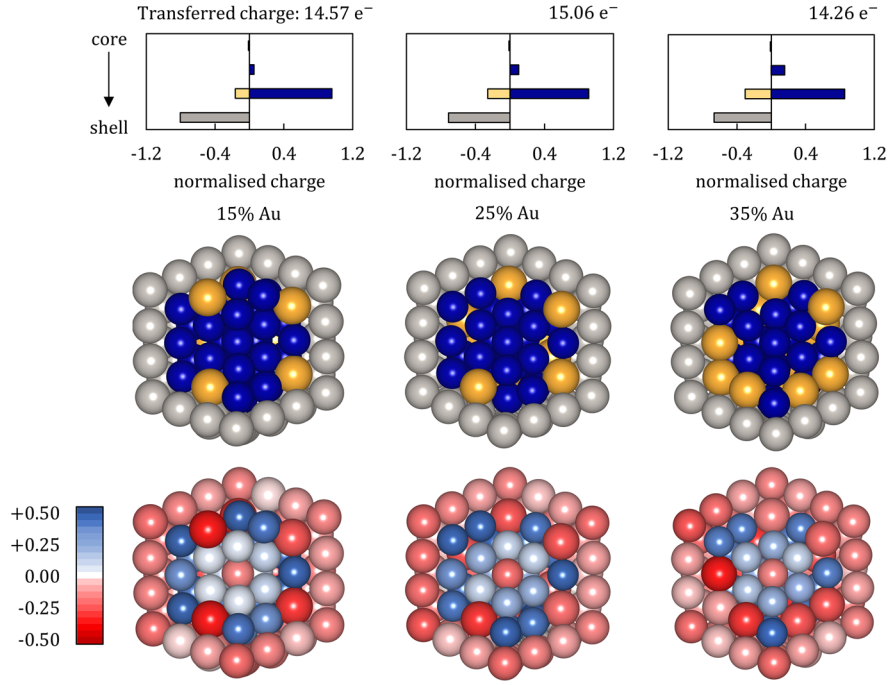

Figure 8. Charge distributions of alloy−core@shell $Pt_{92}(CoAu)_{55}$ NPs with different percentage of Co−Au core alloying (15% Au left, 25% Au middle, 35% Au right). For a detailed description of charge analysis, see Figure 1. Gray, blue, and yellow atoms represent platinum, cobalt, and gold. Legend for charge distribution is given on the bottom left in e^-.

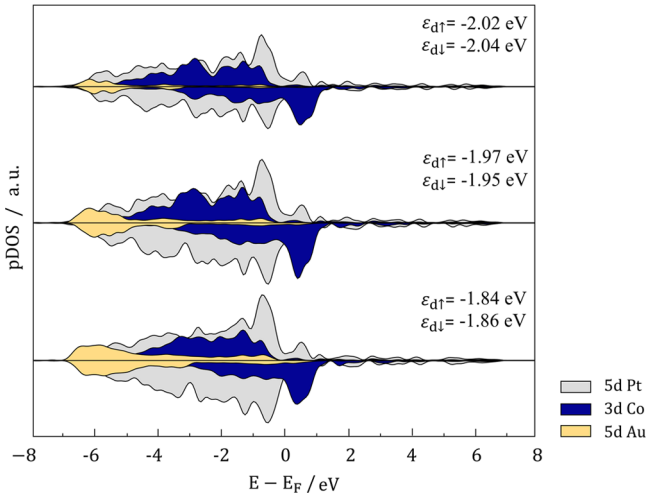

Figure 9. Projected density of states (in a.u.) of alloy−core@shell $Pt_{92}(CoAu)_{55}$ NPs with different percentage of Co−Au core alloying (15% Au top, 25% Au middle, 35% Au bottom). Accompanying d-band center energies are listed in top right corners.

distribution of remaining Co and Pt atoms in the subshell, which plays a significant role in the segregation and adsorption behavior, while the estimate was made considering only one of the many possible layouts. It can therefore be concluded that the coverages of oxygen required for Co surface segregation are very sensitive to the type of nanoparticle. However, in all three cases, segregation is significantly accelerated by the presence of oxidizing species.

In the potential region with the highest ORR activity, but also considering the effect of the potential on the loss of the catalyst surface area (0.60 eV < E < 0.80 eV),[73,74] the observed coverage of adsorbed oxygen on platinum fuel cell cathodes rarely exceeds 0.15 ML, even in the case of PtFe and PtNi catalysts.[75−77] From the DFT predicted O coverages required for Co segregation in the $Pt_{134}Co_{13}$, $Pt_{117}Co_{30}$, and $Pt_{92}Co_{55}$ NPs, only the first two showed respectable stability within the conditions of the experimentally measured ORR oxygen saturation.

In the case of exceptionally high concentrations of oxygen or when certain areas of the NP are in the contact with the support and unavailable to the adsorbates, higher coverages of oxygen per single (111) facet could be expected, in which case the segregation might be triggered even earlier. To account for this situation, segregation with two and three O atoms adsorbed per single segregated Co atom has been modeled for $Pt_{134}Co_{13}$ and $Pt_{92}Co_{55}$ compositions, shown for the latter in Figure 4. Additional oxygen atoms were also adsorbed in the hollow positions, but in such a way to minimize their repulsion. With two and three O atoms adsorbed, ΔE_{seg} is lowered to −0.717 and −1.527 eV for $Pt_{134}Co_{13}$, and to −1.130 and −2.160 eV for the $Pt_{92}Co_{55}$ system, respectively. For both compositions, each addition of oxygen atom causes a more than 2-fold reduction in the segregation energy. Consequently, if oxygen coverage per (111) facet of PtCo NP increases, the overall number of adsorbate atoms needed for the segregation of 13 or 20 Co atoms will drop. However, as the values of ΔE_{seg} for both $Pt_{134}Co_{13}$ and $Pt_{92}Co_{55}$ recede in a similar manner, it can be concluded that the relationship between NPs with different Co concentration will remain the same as with one O atom adsorbed per (111) facet and, therefore, multifold increase in the number of oxygen atoms adsorbed per Co atom was not modeled.

$Pt_{134}Co_{13}$ and $Pt_{117}Co_{30}$ in-core homotops are thermodynamically stable in both vacuum and in an ORR oxygen-rich environment. $Pt_{92}Co_{55}$ NP, however, is expected to be stable as the $Co_{in\text{-}core}$ homotop only in vacuum. The bound oxygen species would facilitate the segregation of core Co atoms under ORR conditions, since adsorption of a single oxygen atom

https://dx.doi.org/10.1021/acs.jpcc.0c04460
J. Phys. Chem. C 2020, 124, 18321−18334

alone is already sufficient to pull a cobalt atom to the surface of the nanoparticle.

3.4. Prediction of Segregation Behavior in Trimetallic PtCoAu Nanoparticles. To improve the thermodynamic stability of the PtCo NPs in the presence of surface-bound oxygen species, Au as a third metal has been introduced to the core−shell compositions considered. Following the works of Zhang et al.[25] and Choi et al.,[36] trimetallic AuCoPt NPs have been modeled in multiple distinctive cases and their chemical and electronical properties have been compared to gain a deeper insight into the effect of gold on both stability and reactivity of PtCo NPs. The focus of this study has been on the $Pt_{92}Co_{55}$ composition, as this system has the lowest Pt loading, thus making it highly preferable, with a few comparison tests conducted on the $Pt_{134}Co_{13}$ system, which is reasonably resistant to segregation even without the addition of the third metal. To tune the segregation energetics, PtCo NPs have first been doped with a reasonable amount of gold, followed by near-surface Au−Co alloying in the core of variable compositions. The two types of NPs have been tested for significant differences.

3.4.1. Doping with Au. Model systems have been doped with a small concentration of Au atoms which were incorporated as part of the Pt shell. In the $Pt_{134}Co_{13}$ NP, 13 Au atoms were positioned in the second Pt layer, making up approximately 23% of the inner part of the nanoparticle. In the interest of comparison of two different PtCo compositions and the role of gold as a dopant, 20 Au atoms were introduced in the Pt shell of the $Pt_{92}Co_{55}$ NP, giving nearly the same concentration of 22% of gold in the outer part of the nanoparticle and leaving the cobalt concentration unchanged. The calculated mixing energy of the correspondingly created $Pt_{121}Co_{13}Au_{13}$ NP is −0.006 eV and of the $Pt_{72}Co_{55}Au_{20}$ NP is −0.230 eV.

Next, the new ternary systems were subjected to the 13 Co atom segregation and oxygen adsorption on $Co_{in\text{-}core}$ and Co_{terr} homotops as was done on the undoped systems; final segregation energy trends are shown in Figure 5 for both the $Pt_{121}Co_{13}Au_{13}$ and $Pt_{92}Co_{55}Au_{20}$ NP. Doping with gold leads to different scenarios in the two systems. While $Pt_{121}Co_{13}Au_{13}$ achieves spontaneous segregation of 13 Co atoms for 27 adsorbed oxygen atoms (∼0.29 ML) − 4 more than if undoped − cobalt segregates more easily in the case of the Au-doped analogue of the $Pt_{92}Co_{55}$ NP and 6 O atoms (∼0.06 ML) are already sufficient whereas 8 were needed in the undoped NP. Thus, the already low oxygen coverage of ∼0.09 ML that was sufficient to trigger Co segregation in the $Pt_{92}Co_{55}$ system and is easily attainable under ORR conditions is furtherly reduced through doping. This outcome is reasonable when the size of Au atoms is considered; as they are slightly larger than Pt atoms, their incorporation in the outer shell induces expansion of existing Pt−Pt bonds making the facets more open, which allows for easier substitution of Pt by Co atoms from the core.

This difference in behavior can also be traced to the electronic properties of these systems. Charge distributions and projected densities of states with d-band center energies are shown in Figure 6. In $Pt_{121}Co_{13}Au_{13}$, gold atoms experience a loss of electrons which makes them positively charged despite their high electronegativity, while in $Pt_{72}Co_{55}Au_{20}$ they accumulate negative charge, although to a lesser extent compared to platinum atoms. Additionally, in the latter case, cobalt atoms in the shell closest to the core atom lose electrons, which mostly results in an overall positive charge, in complete contrast to the undoped system. The charge of Co atoms almost remains constant after doping of the $Pt_{134}Co_{13}$ NP. When combined, this charge distribution makes cobalt atoms less likely to separate in the case of the $Pt_{121}Co_{13}Au_{13}$ NP, but more likely to emerge to the surface and interact with oxidizing species when the composition is that of the $Pt_{72}Co_{55}Au_{20}$ NP. Density of states analysis further supports this view, illustrating that trimetallic hybridization affects the d-band center−and therefore the reactivity toward oxygen atoms−differently, depending on the composition. The average energy of the d-band is increased or decreased through the narrowing or widening of the band, owing to the combination of strain and ligand effects imposed by a combination of metal atoms, to maintain a constant d-band filling.[15] Addition of gold moved both up- and down-spin d-band center energies of the $Pt_{121}Co_{13}Au_{13}$ NP by ∼0.15 eV to more positive values, from −2.14 and −2.02 eV to −1.89 and −1.76 eV, respectively. In the $Pt_{92}Co_{55}Au_{20}$ NP, however, the d-band center remained almost unchanged, with the up-spin energy moving from −2.23 eV to −2.21 eV, and, surprisingly, the down-spin energy decreasing from −2.21 eV to a more negative value of −2.24 eV, at the same time increasing the reactivity.

3.4.2. Alloying with Au. Another possible geometry for the addition of gold as a third metal is the alloy−core@shell NP. This model has been created through the substitution of Co atoms in the subshell of the $Pt_{92}Co_{55}$ NP by Au atoms. To see if the segregation behavior can be tuned by varying the alloy−core composition, three different amounts of Au in the Co core have been tested: ∼15, 25, and 35%, giving $Pt_{92}Co_{47}Au_{8}$, $Pt_{92}Co_{42}Au_{13}$, and $Pt_{92}Co_{36}Au_{19}$ systems with mixing energies of −0.199 eV, −0.156 eV, and −0.105 eV, in that order. For validation of the thermodynamic stability of the core-alloy NPs, their stabilities were compared to the doped counterparts with the same concentrations of Au. Differences in the energy of 0.024 eV for 15% of Au, 0.038 eV for 25% of Au, and 0.071 eV for 35% of Au in favor of doped NPs were detected. However, the difference in the stability was found to reduce with the increase in size of the NPs, giving that the doped 55-atom icosahedral NPs with 15, 25, and 35% of gold were calculated to be more stable than alloy−core 55-atom NPs by 0.033, 0.050, and 0.082 eV, respectively. In addition, despite the apparent thermodynamic disadvantage over doping, many experimental techniques have in recent years been developed for monolayer deposition over the alloyed nanoparticle core, even for the cases where the elements of bigger atomic sizes and low surface energies such as gold were integral components of the alloy. Hence, the constructed alloy−core NPs are considered to make viable models of a possible geometric structure of the catalyst.[25,78−84]

Structures of Co_{terr} homotops were built on the same principle as in previous models, with all Au atoms remaining within the core of the nanoparticle. Segregation energies of $Co_{in\text{-}core}$ and Co_{terr} homotops were calculated and are presented in Figure 7 for $Pt_{92}(CoAu)_{55}$ with different CoAu alloy compositions. NPs with any Co−Au ratio show improved segregation behavior in both vacuum and oxidizing environment. There is a uniform trend of an increase in the number of adsorbed oxygen atoms required to trigger spontaneous segregation as the gold concentration of the alloy−core is increased: instead of the initial 8 oxygen atoms needed for the system with a pure Co core, alloy−core@shell NPs now require 12 (∼0.13 ML), 15 (∼0.16 ML), and 17 atoms (∼0.19

https://dx.doi.org/10.1021/acs.jpcc.0c04460
J. Phys. Chem. C 2020, 124, 18321−18334

ML) of the oxidizing adsorbate in the case of 15, 25, and 35% concentration of Au, respectively. These values are at the upper limit of the oxygen coverages measured on the Pt catalysts in ORR experiments.

Charge distributions arising from Co−Au core alloying are depicted in Figure 8. The overall charge transferred from cobalt atoms varies only slightly for different alloy−core compositions, however, with the increase in the Au concentration the transfer of electrons to gold atoms also increases. Pt atoms, therefore, hold an approximately constant amount of negative charge and, in contrast to the doped system, retain a lower charge compared to the Au atoms. Segregation of Co atoms from the core to the outer shell in any of the alloyed systems causes increased loss of electrons to Pt atoms, leaving their reactivity toward oxygen atoms diminished. The same can be concluded from Figure 9 where the projected densities of state show a uniform increase in the d-band center energies of both up- and down-spin d states, changing to −2.02 and −2.04 eV for 15% of Au, −1.97 and −1.95 eV for 25% of Au, and finally to −1.84 and −1.86 eV for 35% of Au.

4. CONCLUSIONS

We have performed a comprehensive DFT investigation of the segregation behavior of PtCo NPs of different compositions ($Pt_{134}Co_{13}$, $Pt_{117}Co_{30}$, $Pt_{92}Co_{55}$) in vacuum and oxygen-rich environment and compared it to systems with gold as a dopant and with gold integrated in the core to create CoAu alloy−core@Pt shell NPs.

Our results suggest stability of all core−shell NPs in vacuum and insignificant changes for very low coverages of oxygen. As the number of adsorbed oxygen atoms grows, the segregation energy barriers are lowered significantly, and the structures of bimetallic and trimetallic catalytic particles could be rearranged relatively easily. In the $Pt_{134}Co_{13}$ and $Pt_{117}Co_{30}$ systems, an oxygen coverage well above those observed under ORR conditions is needed for the segregation of multiple Co atoms to happen. However, in the $Pt_{92}Co_{55}$ NP, the surface segregation of Co atoms becomes thermodynamically viable with less than one oxygen atom adsorbed per segregated Co atom. As such a low coverage is sufficient to segregate cobalt into the shell, the durability of $Pt_{92}Co_{55}$ NPs would be seriously degraded under ORR conditions via electrochemical dissolution of the segregated Co atoms.

Addition of gold as a dopant has different effects in $Pt_{134}Co_{13}$ and $Pt_{92}Co_{55}$ NPs, as it increases the resistance to segregation for the former but lowers the segregation barrier for the latter. On the basis of our results, this difference in behavior is ascribed to the difference in the electronic properties of Au atoms as they move the d-band center toward more positive values in $Pt_{134}Co_{13}$ doped NPs, and to more negative values in $Pt_{92}Co_{55}$ doped NPs. However, if gold is added to the core of the $Pt_{92}Co_{55}$ NP such that the nanoparticle's core becomes a CoAu alloy, segregation of Co is inhibited. As the concentration of Au in the alloy increases, the barrier for segregation grows in a steady manner, with 35% of Au almost doubling the coverage of oxygen needed for segregation compared to the system without gold. However, as the favorability of mixing energies reduces significantly with the increase in the concentration of gold, the system with 25% of Au has the best properties when subjected to higher coverages of oxygen.

Finally, even though the use of gold to stabilize fuel cell Pt nanocatalyts for the ORR has shown to be an interesting strategy, developing nanocomposites that can lower both Pt and Au usage, through the use of nonprecious metals, while maintaining activity and stability requirements, remains a challenge.

AUTHOR INFORMATION

Corresponding Authors

Glenn Jones − *Johnson Matthey Technology Center, Reading RG4 9NH, U.K.*; Email: gjones@matthey.com

Nora H. de Leeuw − *School of Chemistry, Cardiff University, Cardiff CF10 3AT, U.K.; School of Chemistry, University of Leeds, Leeds LS2 9JT, U.K.*; orcid.org/0000-0002-8271-0545; Email: n.h.deleeuw@leeds.ac.uk

Authors

Barbara Farkaš − *School of Chemistry, Cardiff University, Cardiff CF10 3AT, U.K.*; orcid.org/0000-0002-8297-1673

Christopher B. Perry − *Johnson Matthey Research Centre, CSIR, Pretoria 0184, South Africa*

Complete contact information is available at: https://pubs.acs.org/10.1021/acs.jpcc.0c04460

Notes

The authors declare no competing financial interest.

Information on the data underpinning the presented results, including how to access them, can be found in the Cardiff University Research Portal at 10.17035/d.2020.0107653692.

ACKNOWLEDGMENTS

We acknowledge the UK Economic and Social Research Council (ESRC Grant No. ES/N013867/1) and the National Research Foundation of South Africa for funding under the Newton Programme. We also acknowledge the Engineering and Physical Sciences Research Council (Grant No. EP/R512503/1) for funding and the School of Chemistry at Cardiff University for financial support for a PhD Research Scholarship for B.F. B.F. is also grateful to Jane Mugo, Hellen Chuma, and Donald Mkhonto from Johnson Matthey Research Centre in Pretoria, South Africa, for valuable discussions. This research was undertaken using the Supercomputing Facilities at Cardiff University operated by ARCCA on behalf of the Cardiff Supercomputing Facility and the HPC Wales and Supercomputing Wales (SCW) projects. We acknowledge the support of the latter, which is part-funded by the European Regional Development Fund (ERDF) via Welsh Government. Via our membership of the UK's HPC Materials Chemistry Consortium, which is funded by EPSRC (EP/L000202/1), this work made use of the facilities of ARCHER, the UK's national high-performance computing service, which is funded by the Office of Science and Technology through EPSRC's High End Computing Programme. We also acknowledge the use of the Centre for High Performance Computing (CHPC) facility of South Africa.

REFERENCES

(1) Boudghene Stambouli, A.; Traversa, E. Fuel Cells, an Alternative to Standard Sources of Energy. *Renewable Sustainable Energy Rev.* **2002**, *6*, 295−304.

(2) O'Hyre, R.; Cha, S.-W.; Collela, W.; Prinz, F. B. *Fuel Cell Fundamentals*; John Wiley & Sons, Inc., 2016.

(3) Barbir, F.; Gómez, T. Efficiency and Economics of Proton Exchange Membrane (PEM) Fuel Cells. *Int. J. Hydrogen Energy* **1997**, *22*, 1027−1037.
(4) Bar-On, I.; Kirchain, R.; Roth, R. Technical Cost Analysis for PEM Fuel Cells. *J. Power Sources* **2002**, *109*, 71−75.
(5) Nordin, N. Limitations of Commercializing Fuel Cell Technologies. *AIP Conf. Proc.* **2010**, *1225*, 498−506.
(6) Carrette, L.; Friedrich, K. A.; Stimming, U. Fuel Cells - Fundamentals and Applications. *Fuel Cells* **2001**, *1*, 5−39.
(7) Nørskov, J. K.; Rossmeisl, J.; Logadottir, A.; Lindqvist, L.; Kitchin, J. R.; Bligaard, T.; Jónsson, H. Origin of the Overpotential for Oxygen Reduction at a Fuel-Cell Cathode. *J. Phys. Chem. B* **2004**, *108*, 17886−17892.
(8) Gasteiger, H. A.; Kocha, S. S.; Sompalli, B.; Wagner, F. T. Activity Benchmarks and Requirements for Pt, Pt-Alloy, and Non-Pt Oxygen Reduction Catalysts for PEMFCs. *Appl. Catal., B* **2005**, *56*, 9−35.
(9) Chen, Z.; Higgins, D.; Yu, A.; Zhang, L.; Zhang, J. A Review on Non-Precious Metal Electrocatalysts for PEM Fuel Cells. *Energy Environ. Sci.* **2011**, *4*, 3167−3192.
(10) Sasaki, K.; Naohara, H.; Cai, Y.; Choi, Y. M.; Liu, P.; Vukmirovic, M. B.; Wang, J. X.; Adzic, R. R. Core-Protected Platinum Monolayer Shell High-Stability Electrocatalysts for Fuel-Cell Cathodes. *Angew. Chem., Int. Ed.* **2010**, *49*, 8602−8607.
(11) Oezaslan, M.; Hasché, F.; Strasser, P. Pt-Based Core-Shell Catalyst Architectures for Oxygen Fuel Cell Electrodes. *J. Phys. Chem. Lett.* **2013**, *4*, 3273−3291.
(12) Wang, D.; Xin, H. L.; Hovden, R.; Wang, H.; Yu, Y.; Muller, D. A.; Disalvo, F. J.; Abruña, H. D. Structurally Ordered Intermetallic Platinum-Cobalt Core-Shell Nanoparticles with Enhanced Activity and Stability as Oxygen Reduction Electrocatalysts. *Nat. Mater.* **2013**, *12*, 81−87.
(13) Wei, G. F.; Liu, Z. P. Towards Active and Stable Oxygen Reduction Cathodes: A Density Functional Theory Survey on Pt_2M Skin Alloys. *Energy Environ. Sci.* **2011**, *4*, 1268−1272.
(14) Sharma, S.; Zeng, C.; Peterson, A. A. Face-Centered Tetragonal (FCT) Fe and Co Alloys of Pt as Catalysts for the Oxygen Reduction Reaction (ORR): A DFT Study. *J. Chem. Phys.* **2019**, *150*, 041704.
(15) Kitchin, J. R.; Nørskov, J. K.; Barteau, M. A.; Chen, J. G. Role of Strain and Ligand Effects in the Modification of the Electronic and Chemical Properties of Bimetallic Surfaces. *Phys. Rev. Lett.* **2004**, *93*, 156801.
(16) Bing, Y.; Liu, H.; Zhang, L.; Ghosh, D.; Zhang, J. Nanostructured Pt-Alloy Electrocatalysts for PEM Fuel Cell Oxygen Reduction Reaction. *Chem. Soc. Rev.* **2010**, *39*, 2184−2202.
(17) Ogasawara, H.; Yu, C.; Liu, Z.; Koh, S.; Strasser, P.; Kaya, S.; Toney, M. F.; Greeley, J.; Anniyev, T.; Nilsson, A.; Nordlund, D.; More, K. Lattice-Strain Control of the Activity in Dealloyed Core−Shell Fuel Cell Catalysts. *Nat. Chem.* **2010**, *2*, 454−460.
(18) Loukrakpam, R.; Luo, J.; He, T.; Chen, Y.; Xu, Z.; Njoki, P. N.; Wanjala, B. N.; Fang, B.; Mott, D.; Yin, J.; Klar, J.; Powell, B.; Zhong, C. J. Nanoengineered PtCo and PtNi Catalysts for Oxygen Reduction Reaction: An Assessment of the Structural and Electrocatalytic Properties. *J. Phys. Chem. C* **2011**, *115*, 1682−1694.
(19) Cui, C.; Gan, L.; Li, H. H.; Yu, S. H.; Heggen, M.; Strasser, P. Octahedral PtNi Nanoparticle Catalysts: Exceptional Oxygen Reduction Activity by Tuning the Alloy Particle Surface Composition. *Nano Lett.* **2012**, *12*, 5885−5889.
(20) Ferreira, P. J.; Shao-Horn, Y.; Chen, S.; Sheng, W.; Yabuuchi, N.; Allard, L. F. Enhanced Activity for Oxygen Reduction Reaction on Pt_3Co Nanoparticles: Direct Evidence of Percolated and Sandwich-Segregation Structures. *J. Am. Chem. Soc.* **2008**, *130*, 13818−13819.
(21) Xu, Q.; Kreidler, E.; He, T. Performance and Durability of PtCo Alloy Catalysts for Oxygen Electroreduction in Acidic Environments. *Electrochim. Acta* **2010**, *55*, 7551−7557.
(22) Noh, S. H.; Seo, M. H.; Seo, J. K.; Fischer, P.; Han, B. First Principles Computational Study on the Electrochemical Stability of Pt-Co Nanocatalysts. *Nanoscale* **2013**, *5*, 8625−8633.
(23) Greeley, J.; Mavrikakis, M. Near-Surface Alloys for Hydrogen Fuel Cell Applications. *Catal. Today* **2006**, *111*, 52−58.
(24) Zhang, X.; Yu, S.; Zheng, W.; Liu, P. Stability of Pt near Surface Alloys under Electrochemical Conditions: A Model Study. *Phys. Chem. Chem. Phys.* **2014**, *16*, 16615−16622.
(25) Zhang, L.; Iyyamperumal, R.; Yancey, D. F.; Crooks, R. M.; Henkelman, G. Design of Pt-Shell Nanoparticles with Alloy Cores for the Oxygen Reduction Reaction. *ACS Nano* **2013**, *7*, 9168−9172.
(26) Ruban, A. V.; Skriver, H. L.; Nørskov, J. K. Surface Segregation Energies in Transition-Metal Alloys. *Phys. Rev. B: Condens. Matter Mater. Phys.* **1999**, *59*, 15990−16000.
(27) Menning, C. A.; Chen, J. G. General Trend for Adsorbate-Induced Segregation of Subsurface Metal Atoms in Bimetallic Surfaces. *J. Chem. Phys.* **2009**, *130*, 174709.
(28) Han, B. C.; Miranda, C. R.; Ceder, G. Effect of Particle Size and Surface Structure on Adsorption of O and OH on Platinum Nanoparticles: A First-Principles Study. *Phys. Rev. B: Condens. Matter Mater. Phys.* **2008**, *77*, 075410.
(29) Han, B. C.; Van Der Ven, A.; Ceder, G.; Hwang, B. J. Surface Segregation and Ordering of Alloy Surfaces in the Presence of Adsorbates. *Phys. Rev. B: Condens. Matter Mater. Phys.* **2005**, *72*, 205409.
(30) Rudi, S.; Teschner, D.; Beermann, V.; Hetaba, W.; Gan, L.; Cui, C.; Gliech, M.; Schlögl, R.; Strasser, P. pH-Induced versus Oxygen-Induced Surface Enrichment and Segregation Effects in Pt-Ni Alloy Nanoparticle Fuel Cell Catalysts. *ACS Catal.* **2017**, *7*, 6376−6384.
(31) Wang, C.; Li, D.; Chi, M.; Pearson, J.; Rankin, R. B.; Greeley, J.; Duan, Z.; Wang, G.; Van Der Vliet, D.; More, K. L.; Markovic, N. M.; Stamenkovic, V. R. Rational Development of Ternary Alloy Electrocatalysts. *J. Phys. Chem. Lett.* **2012**, *3*, 1668−1673.
(32) Noh, S. H.; Han, B.; Ohsaka, T. First-Principles Computational Study of Highly Stable and Active Ternary PtCuNi Nanocatalyst for Oxygen Reduction Reaction. *Nano Res.* **2015**, *8*, 3394−3403.
(33) Heggen, M.; Gocyla, M.; Dunin-Borkowski, R. E. The Growth and Degradation of Binary and Ternary Octahedral Pt−Ni-Based Fuel Cell Catalyst Nanoparticles Studied Using Advanced Transmission Electron Microscopy. *Adv. Phys. X* **2017**, *2*, 281−301.
(34) Mani, P.; Srivastava, R.; Strasser, P. Dealloyed Binary PtM_3 (M = Cu, Co, Ni) and Ternary $PtNi_3M$ (M = Cu, Co, Fe, Cr) Electrocatalysts for the Oxygen Reduction Reaction: Performance in Polymer Electrolyte Membrane Fuel Cells. *J. Power Sources* **2011**, *196*, 666−673.
(35) Tripkovic, V.; Hansen, H. A.; Rossmeisl, J.; Vegge, T. First Principles Investigation of the Activity of Thin Film Pt, Pd and Au Surface Alloys for Oxygen Reduction. *Phys. Chem. Chem. Phys.* **2015**, *17*, 11647−11657.
(36) Choi, J.; Cho, J.; Roh, C. W.; Kim, B. S.; Choi, M. S.; Jeong, H.; Ham, H. C.; Lee, H. Au-Doped PtCo/C Catalyst Preventing Co Leaching for Proton Exchange Membrane. *Appl. Catal., B* **2019**, *247*, 142−149.
(37) Kresse, G.; Furthmüller, J. Efficiency of Ab-Initio Total Energy Calculations for Metals and Semiconductors Using a Plane-Wave Basis Set. *Comput. Mater. Sci.* **1996**, *6*, 15−50.
(38) Perdew, J. P.; Burke, K.; Ernzerhof, M. Generalized Gradient Approximation Made Simple. *Phys. Rev. Lett.* **1996**, *77*, 3865−3868.
(39) Yang, K.; Zheng, J.; Zhao, Y.; Truhlar, D. G. Tests of the RPBE, RevPBE, τ-HCTHhyb, ωb97X-D, and MOHLYP Density Functional Approximations and 29 Others against Representative Databases for Diverse Bond Energies and Barrier Heights in Catalysis. *J. Chem. Phys.* **2010**, *132*, 164117.
(40) Teng, B. T.; Wen, X. D.; Fan, M.; Wu, F. M.; Zhang, Y. Choosing a Proper Exchange-Correlation Functional for the Computational Catalysis on Surface. *Phys. Chem. Chem. Phys.* **2014**, *16*, 18563−18569.
(41) Matanović, I.; Garzon, F. H.; Henson, N. J. Theoretical Study of Electrochemical Processes on Pt-Ni Alloys. *J. Phys. Chem. C* **2011**, *115*, 10640−10650.

https://dx.doi.org/10.1021/acs.jpcc.0c04460
J. Phys. Chem. C 2020, 124, 18321−18334

(42) Front, A.; Legrand, B.; Tréglia, G.; Mottet, C. Bidimensional Phases in Co−Pt Surface Alloys: A Theoretical Study of Ordering and Surface Segregation. *Surf. Sci.* **2019**, *679*, 128−138.
(43) Hirunsit, P.; Balbuena, P. B. Surface Atomic Distribution and Water Adsorption on Pt-Co Alloys. *Surf. Sci.* **2009**, *603*, 912−920.
(44) Kootte, A.; Haas, C.; De Groot, R. A. The Electronic Structure of Ordered Binary Co-Pt Compounds. *J. Phys.: Condens. Matter* **1991**, *3*, 1133−1152.
(45) Darling, A. S. Cobalt-Platinum Alloys. *Johnson Matthey Technol. Rev.* **1963**, *3*, 96−104.
(46) Kittel, C. *Introduction to Solid State Physics*; John Wiley & Sons, Inc., 2010.
(47) Niessen, A. K.; Miedema, A. R.; de Boer, F. R.; Boom, R. Enthalpies of Formation of Liquid and Solid Binary Alloys Based on 3d Metals. IV. Alloys of Cobalt. *Phys. B+C* **1988**, *151*, 401−432.
(48) Cyr, J. P.; Dellacherle, J.; Balesdent, D. Critical Evaluation of Thermodynamic Properties of Mixing for Solid Cobalt-Platinum Alloys between 1000 and 1400 K. *J. Chem. Eng. Data* **1981**, *26*, 174−178.
(49) Oriani, R. A. Thermodynamics of Ordering Alloys, I. Activities in Cobalt-Platinum Alloys and Some General Considerations on Ordering Systems. *Acta Metall.* **1953**, *1*, 144−152.
(50) Kresse, G.; Joubert, D. From Ultrasoft Pseudopotentials to the Projector Augmented-Wave Method. *Phys. Rev. B: Condens. Matter Mater. Phys.* **1999**, *59*, 1758−1775.
(51) Grimme, S.; Ehrlich, S.; Goerigk, L. Effect of the Damping Function in Dispersion Corrected Density Functional Theory. *J. Comput. Chem.* **2011**, *32*, 1456−1465.
(52) Jellinek, J.; Krissinel, E. B. Ni_nAl_m Alloy Clusters: Analysis of Structural Forms and Their Energy Ordering. *Chem. Phys. Lett.* **1996**, *258*, 283−292.
(53) Ferrando, R.; Jellinek, J.; Johnston, R. L. Nanoalloys: From Theory to Applications of Alloy Clusters and Nanoparticles. *Chem. Rev.* **2008**, *108*, 845−910.
(54) Shi, H.; Stampfl, C. First-Principles Investigations of the Structure and Stability of Oxygen Adsorption and Surface Oxide Formation at Au(111). *Phys. Rev. B: Condens. Matter Mater. Phys.* **2007**, *76*, 075327.
(55) Li, W.-X.; Stampfl, C.; Scheffler, M. Oxygen Adsorption on Ag(111): A Density-Functional Theory Investigation. *Phys. Rev. B: Condens. Matter Mater. Phys.* **2002**, *65*, 075407.
(56) Rossini, F. D. *JANAF Thermochemical Tables*; American Institute of Physics: New York, 1972.
(57) Henkelman, G.; Arnaldsson, A.; Jónsson, H. A Fast and Robust Algorithm for Bader Decomposition of Charge Density. *Comput. Mater. Sci.* **2006**, *36*, 354−360.
(58) Tsai, H.-C.; Yu, T. H.; Sha, Y.; Merinov, B. V.; Wu, P.-W.; Chen, S.-Y.; Goddard, W. A. Density Functional Theory Study of Pt_3M Alloy Surface Segregation with Adsorbed O/OH and Pt_3Os as Catalysts for Oxygen Reduction Reaction. *J. Phys. Chem. C* **2014**, *118*, 26703−26712.
(59) Tafreshi, S. S.; Roldan, A.; Dzade, N. Y.; De Leeuw, N. H. Adsorption of Hydrazine on the Perfect and Defective Copper (111) Surface: A Dispersion-Corrected DFT Study. *Surf. Sci.* **2014**, *622*, 1−8.
(60) Verga, L. G.; Aarons, J.; Sarwar, M.; Thompsett, D.; Russell, A. E.; Skylaris, C. K. DFT Calculation of Oxygen Adsorption on Platinum Nanoparticles: Coverage and Size Effects. *Faraday Discuss.* **2018**, *208*, 497−522.
(61) Viswanathan, V.; Wang, F. Y. F. Theoretical Analysis of the Effect of Particle Size and Support on the Kinetics of Oxygen Reduction Reaction on Platinum Nanoparticles. *Nanoscale* **2012**, *4*, 5110−5117.
(62) Shao, M.; Peles, A.; Shoemaker, K. Electrocatalysis on Platinum Nanoparticles: Particle Size Effect on Oxygen Reduction Reaction Activity. *Nano Lett.* **2011**, *11*, 3714−3719.
(63) Wei, G. F.; Liu, Z. P. Optimum Nanoparticles for Electrocatalytic Oxygen Reduction: The Size, Shape and New Design. *Phys. Chem. Chem. Phys.* **2013**, *15*, 18555−18561.
(64) Tan, T. L.; Wang, L. L.; Zhang, J.; Johnson, D. D.; Bai, K. Platinum Nanoparticle during Electrochemical Hydrogen Evolution: Adsorbate Distribution, Active Reaction Species, and Size Effect. *ACS Catal.* **2015**, *5*, 2376−2383.
(65) Shao, M.; Chang, Q.; Dodelet, J. P.; Chenitz, R. Recent Advances in Electrocatalysts for Oxygen Reduction Reaction. *Chem. Rev.* **2016**, *116*, 3594−3657.
(66) Miyatake, K.; Shimizu, Y. Pt/Co Alloy Nanoparticles Prepared by Nanocapsule Method Exhibit a High Oxygen Reduction Reaction Activity in the Alkaline Media. *ACS Omega* **2017**, *2*, 2085−2089.
(67) Zhao, Y.; Liu, J.; Zhao, Y.; Wang, F. Composition-Controlled Synthesis of Carbon-Supported Pt-Co Alloy Nanoparticles and the Origin of Their ORR Activity Enhancement. *Phys. Chem. Chem. Phys.* **2014**, *16*, 19298−19306.
(68) Escaño, M. C. S. First-Principles Calculations of the Dissolution and Coalescence Properties of Pt Nanoparticle ORR Catalysts: The Effect of Nanoparticle Shape. *Nano Res.* **2015**, *8*, 1689−1697.
(69) Guedes-Sobrinho, D.; Freire, R. L. H.; Chaves, A. S.; Da Silva, J. L. F. Ab Initio Investigation of the Role of CO Adsorption on the Physical Properties of 55-Atom PtCo Nanoalloys. *J. Phys. Chem. C* **2017**, *121*, 27721−27732.
(70) Kettner, M.; Schneider, W. B.; Auer, A. A. Computational Study of Pt/Co Core-Shell Nanoparticles: Segregation, Adsorbates and Catalyst Activity. *J. Phys. Chem. C* **2012**, *116*, 15432−15438.
(71) Farkaš, B.; Santos-Carballal, D.; Cadi-Essadek, A.; de Leeuw, N. H. A DFT+U Study of the Oxidation of Cobalt Nanoparticles: Implications for Biomedical Applications. *Materialia* **2019**, *7*, 100381.
(72) Lynch, M.; Hu, P. Density Functional Theory Study of CO and Atomic Oxygen Chemisorption on Pt(111). *Surf. Sci.* **2000**, *458*, 1−14.
(73) Tian, F.; Anderson, A. B. Effective Reversible Potential, Energy Loss, and Overpotential on Platinum Fuel Cell Cathodes. *J. Phys. Chem. C* **2011**, *115*, 4076−4088.
(74) Borup, R. L.; Davey, J. R.; Garzon, F. H.; Wood, D. L.; Inbody, M. A. PEM Fuel Cell Electrocatalyst Durability Measurements. *J. Power Sources* **2006**, *163*, 76−81.
(75) Marković, N. M.; Stamenkovic, V. R.; Fowler, B.; Mun, B. S.; Wang, G. Activity on Pt_3Ni (111) via Increased Surface Site Availability. *Science.* **2007**, *315*, 493−497.
(76) Wakisaka, M.; Suzuki, H.; Mitsui, S.; Uchida, H.; Watanabe, M. Increased Oxygen Coverage at Pt-Fe Alloy Cathode for the Enhanced Oxygen Reduction Reaction Studied by EC-XPS. *J. Phys. Chem. C* **2008**, *112*, 2750−2755.
(77) Casalongue, H. S.; Kaya, S.; Viswanathan, V.; Miller, D. J.; Friebel, D.; Hansen, H. A.; Nørskov, J. K.; Nilsson, A.; Ogasawara, H. Direct Observation of the Oxygenated Species during Oxygen Reduction on a Platinum Fuel Cell Cathode. *Nat. Commun.* **2013**, *4*, 2817.
(78) Zhang, J.; Lima, F. H. B.; Shao, M. H.; Sasaki, K.; Wang, J. X.; Hanson, J.; Adzic, R. R. Platinum Monolayer on Nonnoble Metal-Noble Metal Core-Shell Nanoparticle Electrocatalysts for O_2 Reduction. *J. Phys. Chem. B* **2005**, *109*, 22701−22704.
(79) Shao, M.; Sasaki, K.; Marinkovic, N. S.; Zhang, L.; Adzic, R. R. Synthesis and Characterization of Platinum Monolayer Oxygen-Reduction Electrocatalysts with Co-Pd Core-Shell Nanoparticle Supports. *Electrochem. Commun.* **2007**, *9*, 2848−2853.
(80) Chen, Y.; Wang, Z.; Chen, X.; Zeng, D.; Li, M.; Peng, D. L. Solution Preparation of Alloy Core−Shell Nanoparticles: The Case of Ni−Cu@Au−Cu Nanoparticles. *Mater. Lett.* **2013**, *99*, 180−183.
(81) Nan, H.; Tian, X.; Luo, J.; Dang, D.; Chen, R.; Liu, L.; Li, X.; Zeng, J.; Liao, S. A Core-Shell $Pd_1Ru_1Ni_2$@Pt/C Catalyst with a Ternary Alloy Core and Pt Monolayer: Enhanced Activity and Stability towards the Oxygen Reduction Reaction by the Addition of Ni. *J. Mater. Chem. A* **2016**, *4*, 847−855.
(82) Yancey, D. F.; Zhang, L.; Crooks, R. M.; Henkelman, G. Au@Pt Dendrimer Encapsulated Nanoparticles as Model Electrocatalysts for Comparison of Experiment and Theory. *Chem. Sci.* **2012**, *3*, 1033−1040.

https://dx.doi.org/10.1021/acs.jpcc.0c04460
J. Phys. Chem. C 2020, 124, 18321−18334

(83) Nan, H.; Tian, X.; Yang, L.; Shu, T.; Song, H.; Liao, S. A Platinum Monolayer Core-Shell Catalyst with a Ternary Alloy Nanoparticle Core and Enhanced Stability for the Oxygen Reduction Reaction. *J. Nanomater.* **2015**, *2015*, 715474.
(84) Li, J.; Sharma, S.; Liu, X.; Pan, Y. T.; Spendelow, J. S.; Chi, M.; Jia, Y.; Zhang, P.; Cullen, D. A.; Xi, Z.; Lin, H.; Yin, Z.; Shen, B.; Muzzio, M.; Yu, C.; Kim, Y. S.; Peterson, A. A.; More, K. L.; Zhu, H.; Sun, S. Hard-Magnet L10-CoPt Nanoparticles Advance Fuel Cell Catalysis. *Joule* **2019**, *3*, 124−135.

https://dx.doi.org/10.1021/acs.jpcc.0c04460
J. Phys. Chem. C 2020, 124, 18321−18334